Time-domain analysis for field excited transmission lines with nonlinear loads

2003 J. Phys. A: Math. Gen. 36 10573

(http://iopscience.iop.org/0305-4470/36/42/011)

INSTITUTE OF PHYSICS PUBLISHING JOURNAL OF PHYSICS A: MATHEMATICAL AND GENERAL

J. Phys. A: Math. Gen. **36** (2003) 10573–10584 PII: S0305-4470(03)63432-3

Time-domain analysis for field excited transmission lines with nonlinear loads

A Maaouni[1] **and A Amri**

Laboratoire d'Electronique, d'Electromagnétisme et d'Hyperfréquences. Université Hassan II, Faculté des Sciences Ain-chock, Casablanca, BP 5336 Maârif, Morocco

Received 7 May 2003, in final form 19 August 2003
Published 7 October 2003
Online at stacks.iop.org/JPhysA/36/10573

Abstract

This paper deals with the study of transients in overhead lines illuminated by an interfering plane-wave disturbance. Simple and accurate analytical expressions for transmission line parameters are used to take into account losses in the ground. Transmission line equations are derived in the Laplace *s*-domain. An FFT-based numerical inverse Laplace transform (FNILT) is used in conjunction with the piecewise decomposition technique to evaluate transient induced currents and voltages at nonlinear line terminals. Sample numerical results are presented.

PACS numbers: 02.30.Nw, 84.40.Az

1. Introduction

The sensitivity of electronic devices in power networks to electromagnetic interferences (EMI) has increased the interest in transients particularly in transmission lines that constitute the fundamental connection elements for electronic and power subsystems. Various approaches have been proposed in the literature [1–4] for the analysis of the field-to-transmission line problems. These methods can be divided into two groups: time-domain [6–8] and frequency-domain methods [1, 3, 5, 9]. When dealing with above-ground multiconductors, it is useful to formulate the problem in the frequency domain. Indeed, in this domain it is easier to carry out equations describing losses in the ground, line propagation effects and the wire-to-wire coupling. The time-domain results are usually obtained using FFT techniques.

A procedure based on transmission-line theory is utilized in this paper. The losses in the ground are taken into account by introducing an accurate, simple and analytical expression for the frequency-dependent line parameters [10]. The proposed formulation obeys the telegraphers equation model, with a substantial difference with respect to other previous works. In fact, the most frequently-used technique for generating the general solution to the multiconductor transmission line equations is based on the application of the modal concept

[1] Present address: Hay Sadri, Rue 10, no 135, Groupe 3, Casablanca, Morocco.

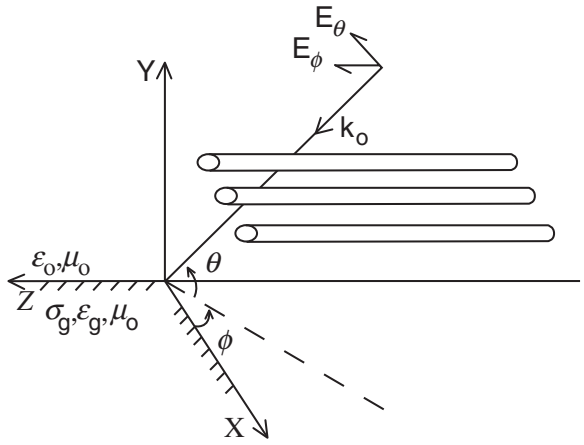

Figure 1. Line geometry.

in the frequency domain. The line equations are uncoupled using transformation matrices to obtain a set of uncoupled equations which could be solved by an inspection method. The Fourier transform is then performed to provide the time-domain solution. In this work, the computation of the admittance matrix relating the terminal currents and voltages of the line is performed in the Laplace s-domain without the need of mode quantities. Furthermore, the line network is divided into frequency-dependent and nonlinear time-dependent parts. The nonlinear line terminals such as surge arresters (varistor, sparkgap) are excited by piecewise linear time-dependent sources. The time-domain response of the frequency-dependent part of the network is achieved using an accurate FFT-based numerical inverse Laplace transform. Then, a Newton–Raphson iteration is stated to include the nonlinear part. Finally, some numerical examples are presented.

2. Formulation in the frequency s-domain

2.1. Transmission line model

The problem considered consists of a system of N conductors, all parallel to the z-axis and located above a lossy earth with electrical parameters $\varepsilon_g = \varepsilon_{rg}\varepsilon_o$, σ_g and μ_o . These conductors are of length l. The region ($y > 0$) is taken to be a free space of electrical constants ε_o, μ_o. The earth (region $y < 0$) is assumed to be homogeneous and a complex refractive index n is defined for it as $n = \left(\varepsilon_{rg} + \frac{\sigma_g}{s\varepsilon_o}\right)^{\frac{1}{2}}$. The nth conductor has a radius of a_n and is located at a height $y = h_n$ and a position $x = d_n$. A plane wave, which is assumed to have an arbitrary polarization, is incident on the line as described by the angles θ and ϕ (see figure 1).

The behaviour of the voltages and currents on an excited N above-ground coupled transmission-line system is described in terms of the telegrapher equations in the frequency s-domain [2, 3]

$$\begin{aligned} &\frac{\mathrm{d}\mathbf{V}^s(z,s)}{\mathrm{d}z} + \mathbf{Z}(s)\mathbf{I}(z,s) = \mathbf{E}_z(\mathbf{d},\mathbf{h},z,s) - \mathbf{E}_z(\mathbf{d},\mathbf{0},z,s) \\ &\frac{\mathrm{d}\mathbf{I}(z,s)}{\mathrm{d}z} + \mathbf{Y}(s)\mathbf{V}^s(z,s) = 0 \qquad (0 < z < l) \end{aligned} \tag{1}$$

where $\mathbf{E}_z$ is the tangential exciting electric field. The scattered voltage $\mathbf{V}^s$ can be expressed in terms of the total voltage $\mathbf{V}$ induced on the line and the exciting voltage $\mathbf{V}^e$

$$\mathbf{V}^s(z,s) = \mathbf{V}(z,s) - \mathbf{V}^e(z,s) = \mathbf{V}(z,s) - \int_{\mathbf{h}}^{\mathbf{0}} \mathbf{E}_y(\mathbf{d}, y, z, s)\,\mathrm{d}y \tag{2}$$

where $\mathbf{E}_y$ is the vertical exciting electric field component. $\mathbf{Z}(s)$ and $\mathbf{Y}(s)$ are $N \times N$-dimensional matrices which represent the series impedance and the shunt admittance per unit length of the line. $\mathbf{V}(z,s)$ and $\mathbf{I}(z,s)$ are column vectors defining the voltages $v_k(z,s)$ and currents $i_k(z,s)$ induced on the conductors $k = 1, 2, 3, \ldots, N$. These voltages are measured by taking the ground plane as a reference conductor $\mathbf{h} = (h_k)_{k=1,\ldots,N}$ and $\mathbf{d} = (d_k)_{k=1,\ldots,N}$. The frequency-dependent distributed parameter line model, characterized by $\mathbf{Z}(s)$ and $\mathbf{Y}(s)$, was directly obtained from scattering theory under quasi-TEM wave propagation. The model takes into account the effects of the finite ground conductivity. Simple and accurate analytical expressions for the line parameters were derived in [10]. Only the final results are quoted here in terms of the inductance matrix $\mathbf{L}$ and the quantities $\mathbf{G}$ and $\mathbf{J}$ which represent, respectively, the losses of the conduction and the displacement current in the ground,

$$\mathbf{Z}(s) = \mathbf{Z}_w(s) + s\left(\mathbf{L} + \frac{\mu_0}{2\pi}\mathbf{J}\right) \tag{3}$$

$$\mathbf{Y}(s) = \frac{s}{v^2}\left(\mathbf{L} + \frac{\mu_0}{2\pi}\mathbf{G}\right)^{-1}. \tag{4}$$

The term $\mathbf{Z}_w$ associated with the conductor internal impedances is a diagonal matrix and a function of s. The internal impedance matrix elements $\mathbf{Z}_{wkl}$ can be easily determined for various conductor types [1]. For thin solid conductors

$$\begin{aligned} \mathbf{Z}_{wkl} &= \frac{\mu_w}{2\pi b_k}\sqrt{s}\frac{I_0(b_k\sqrt{s})}{I_1(b_k\sqrt{s})}\delta_{kl} \\ \delta_{kl} &= \begin{cases} 1, & k = l \\ 0, & k \neq l \end{cases} \qquad (k, l = 1, 2, \ldots, N) \end{aligned} \tag{5}$$

where $b_k = a_k\sqrt{\sigma_w\mu_w}$, with μ_w and σ_w being the electrical parameters characterizing the kth wire. $I_0(z)$ and $I_1(z)$ are the modified Bessel functions.

The elements of the external inductance matrix which do not depend on s (the quasi-stationary approximation) are

$$\mathbf{L}_{kl} = \frac{\mu_0}{2\pi}\ln\left(\frac{\sqrt{((d_k - d_l)^2 + (h_l + h_k)^2)}}{\sqrt{((d_k - d_l)^2 + (h_l - h_k)^2)}}\right) \qquad (k, l = 1, 2, \ldots, N). \tag{6}$$

The contribution of losses in the ground is specified by the matrices $\mathbf{G}$ and $\mathbf{J}$ whose elements are [10]

$$\begin{aligned} \mathbf{J}_{kl} &= \ln\left(\frac{\sqrt{(d_k - d_l)^2 + (h_l + h_k + 2/(k_0\sqrt{1-n^2}))^2}}{\sqrt{((d_k - d_l)^2 + (h_l + h_k)^2)}}\right) \\ \mathbf{G}_{kl} &= P(\Omega_{kl}) + P(\bar{\Omega}_{kl}) \qquad (k, l = 1, 2, \ldots, N) \end{aligned} \tag{7}$$

where $\Omega_{kl} = k_0(h_k + h_l + \mathbf{i}\,|d_k - d_l|)$, $\bar{\Omega}_{kl} = k_0(h_k + h_l - \mathbf{i}\,|d_k - d_l|)$ and

$$P(z) = \left(-\frac{1}{4} + \frac{1}{2}\frac{1}{n^2+1}\right)Q(bz) + \frac{1}{4}Q\left(bz + \frac{2b}{\sqrt{n^2-1}}\right) - \frac{1}{2}\ln\left(1 + \frac{2}{\sqrt{1-n^2}}\right) \tag{8}$$

with $Q(z) = \exp(-z)\mathbf{E}_1(-z) + \exp(z)\mathbf{E}_1(z)$. The exponential integral is defined by $\mathbf{E}_1(z) = \int_z^\infty \exp(-t)/t\,\mathrm{d}t$ [11, p 228], and $b = \mathbf{i}/\sqrt{n^2+1}$. $k_0 = \mathbf{i}\,s/v$ is the propagation constant in air. v is the speed of light in air.

2.2. Exciting electric field

In determining the response of the multiconductor line subjected to an external excitation, it is first necessary to evaluate the impressed tangential electric field on the conductors and the vertical exciting electric field component. Because the external excitation is assumed to be an electromagnetic EMP plane wave propagating in the free space at speed v , the incident and the ground-reflected electric fields are described by the following expressions,

$$\mathbf{E}^+(\mathbf{r}, s) = \mathbf{P}^+ E(s)\,\mathrm{e}^{\mathbf{i}\mathbf{k}_o^+\mathbf{r}} \tag{9}$$

$$\mathbf{E}^-(\mathbf{r}, s) = (\Gamma_v \mathbf{P}_v^- + \Gamma_h \mathbf{P}_h^-) E(s)\,\mathrm{e}^{\mathbf{i}\mathbf{k}_o^-\mathbf{r}} \tag{10}$$

where $\mathbf{r} = x\mathbf{i}_x + y\mathbf{i}_y + z\mathbf{i}_z$ is the position vector and $E(s)$ is the Laplace transform of the impulse waveform. $\mathbf{P}^\pm = (\cos(\eta)\mathbf{a}_\theta^\pm + \sin(\eta)\mathbf{a}_\phi)$. $\mathbf{P}^+$ is the polarization unit vector of the incident electric field $\mathbf{E}^+$ and η is the polarization angle. It is useful to note that for the vertically polarized incident field $\eta = 0^\circ$ ($\mathbf{P}^+$ lies in the incidence plane). The horizontally polarized part of the incident field is obtained by taking $\eta = 90^\circ$ ($\mathbf{P}^+$ is perpendicular to the incidence plane). The subscripts v and h designate the vertical and the horizontal polarizations respectively. In a Cartesian coordinate system

$$\begin{aligned} \mathbf{a}_\theta^\pm &= \mp\sin(\theta)\sin(\phi)\mathbf{i}_x + \cos(\theta)\mathbf{i}_y \pm \sin(\theta)\cos(\phi)\mathbf{i}_z \\ \mathbf{a}_\phi &= \cos(\phi)\mathbf{i}_x + \sin(\phi)\mathbf{i}_z \end{aligned} \tag{11}$$

$$\begin{aligned} \mathbf{k}_o^\pm &= \frac{\mathbf{i}\,s}{v}(-\cos(\theta)\sin(\phi)\mathbf{i}_x \mp \sin(\theta)\mathbf{i}_y + \cos(\theta)\cos(\phi)\mathbf{i}_z) \\ \mathbf{P}^- &= \mathbf{P}_v^- + \mathbf{P}_h^- \qquad \mathbf{P}_v^- = \cos(\eta)\mathbf{a}_\theta^- \qquad \mathbf{P}_h^- = \sin(\eta)\mathbf{a}_\phi. \end{aligned} \tag{12}$$

The terms Γ_v and Γ_h are the vertical and the horizontal Fresnel reflection coefficients for a lossy earth. These are expressed as [12]

$$\begin{aligned} \Gamma_v &= \frac{n^2\sin(\theta) - \sqrt{n^2 - \cos(\theta)^2}}{n^2\sin(\theta) + \sqrt{n^2 - \cos(\theta)^2}} \\ \Gamma_h &= \frac{\sin(\theta) - \sqrt{n^2 - \cos(\theta)^2}}{\sin(\theta) + \sqrt{n^2 - \cos(\theta)^2}}. \end{aligned} \tag{13}$$

The resultant electric field affecting the line conductors is obtained by summing (9) and (10),

$$\mathbf{E}(\mathbf{r}, s) = \mathbf{E}^+(\mathbf{r}, s) + \mathbf{E}^-(\mathbf{r}, s). \tag{14}$$

Note that in equations (9), (10) and (14), the zero phase is at the origin of a Cartesian coordinate system at $\mathbf{r} = \mathbf{0}$, which implies that the EMP plane wave impinging on the air–earth interface reaches this point at $t = 0$. A simple manipulation of (9), (10), (11) and (14) can be performed to yield the y- and z-directed components of the total electric field at a position denoted by (x, y, z) as

$$\begin{aligned} E_z = E(s)\Big[&(\cos(\eta)\sin(\theta)\cos(\phi) + \sin(\eta)\sin(\phi))\exp\left(\frac{s}{v}\sin(\theta)y\right) \\ &+ (\Gamma_v\cos(\eta)\sin(\theta)\cos(\phi) - \Gamma_h\sin(\eta)\sin(\phi))\exp\left(-\frac{s}{v}\sin(\theta)y\right)\Big] \\ &\times\exp\left(-\frac{s}{v}(-\cos(\theta)\sin(\phi)x + \cos(\theta)\cos(\phi)z)\right) \end{aligned} \tag{15}$$

$$E_y = E(s)\cos(\eta)\cos(\theta)\left[\exp\left(\frac{s}{v}\sin(\theta)y\right) + \Gamma_v \exp\left(-\frac{s}{v}\sin(\theta)y\right)\right] \times \exp\left(-\frac{s}{v}(-\cos(\theta)\sin(\phi)x + \cos(\theta)\cos(\phi)z)\right). \quad (16)$$

3. Nonlinear loaded line equations

3.1. Piecewise linear approximation

When dealing with lightning overvoltages, it is usual to employ nonlinear devices to clip and limit high amplitude overvoltages and currents which can occur on a multiconductor line system. In this paper, time-dependent nonlinear resistances (varistors) are used as nonlinear line terminations. It is assumed that nonlinear models are static and voltage-controlled current sources (VCCS). The nonlinear voltage-controlled current source may be expressed as a function of voltages $\mathbf{I}(\tau) = \mathbf{f}(\mathbf{V}(\tau))$. By the word static it is meant that function $\mathbf{f}$ depends only on the instantaneous values of the voltages.

By decomposing the nonlinear VCCS $\mathbf{I}(\tau)$ as a sum of say M terms

$$\mathbf{I}(\tau) = \sum_{k=0}^{M-1} \mathbf{I}^k(\tau)$$

the response $\boldsymbol{\chi}(\tau)$ of a linear network at time τ may be calculated as the sum of the responses due to each of the $\mathbf{I}^k(.)$ acting alone

$$\boldsymbol{\chi}(\tau) = \sum_{k=0}^{M-1} \boldsymbol{\chi}^k(\tau) + \boldsymbol{\chi}_s(\tau)$$

where $\boldsymbol{\chi}^k$ is the response of the network obtained while replacing nonlinear ports by the time-dependent current source $\mathbf{I}^k(.)$. Note that when all $\mathbf{I}^k$ are set to zero, $\boldsymbol{\chi} = \boldsymbol{\chi}_s$.

Now, let us approximate $\mathbf{I}(\tau)$ by first dividing the analysis interval $[0, T]$ into M intervals of length Δ, that is $\Delta = \frac{T}{M}$, and second, over each successive interval, say (τ_k, τ_{k+1}), we replace the curve $\mathbf{I}(\tau)$ by a linear segment for $\tau_k < \tau < \tau_k + \Delta = \tau_{k+1}$. Thus, it is clear that the linear-piecewise approximation of the nonlinear VCCS may be described by the following relationship:

$$\mathbf{I}(\tau) = \sum_{k=0}^{M-1} (\mathbf{I}_{Ak}\tau + \mathbf{I}_{Bk}) P_\Delta(\tau - \tau_k) \qquad (0 < \tau < T) \quad (17)$$

where P_Δ is the rectangular pulse. This is expressed in terms of the unit step function $H(.)$ as: $P_\Delta(\tau) = \frac{1}{\Delta}(H(\tau) - H(\tau - \Delta))$,

$$\mathbf{I}_{Ak} = \mathbf{I}_{k+1} - \mathbf{I}_k \qquad \mathbf{I}_k = \mathbf{I}(\tau_k) \qquad \mathbf{I}_{Bk} = \Delta\mathbf{I}_k - (\mathbf{I}_{k+1} - \mathbf{I}_k)\tau_k.$$

3.2. Resolution of coupling equations in the Laplace s-domain

Now, consider the situation described in figure 2 to illustrate the formulation of transmission line coupling equations. An uniform two-wire transmission line whose conductors are located at ($d_1 = 0\,\text{m}, h_1 = 5\,\text{m}$) and ($d_2 = 2\,\text{m}, h_1 = 5\,\text{m}$) and both have a radius of $a_1 = a_2 = 2.5\,\text{mm}$. Each wire is terminated at the far end ($z = l$) by a nonlinear resistor and at the near end ($z = 0$) by a resistor R. The length of the line is taken to be $l = 10\,\text{m}$. The line is illuminated by a plane wave. We now return to the general formulation.

On inserting equation (2) in (1), it is easy to show that

$$\frac{\mathrm{d}\boldsymbol{\Psi}(z,s)}{\mathrm{d}z} + \mathbf{A}(s)\boldsymbol{\Psi}(z,s) = \boldsymbol{\Psi}_s(z,s) \tag{18}$$

where $\boldsymbol{\Psi}(z,s) = (v_1(z,s), v_2(z,s), \ldots, v_N(z,s), i_1(z,s), i_2(z,s), \ldots, i_N(z,s))^T$ and

$$\mathbf{A}(s) = \begin{pmatrix} \mathbf{0} & \mathbf{Z}(s) \\ \mathbf{Y}(s) & \mathbf{0} \end{pmatrix}. \tag{19}$$

The superscript T designates the transpose. The column vector $\boldsymbol{\Psi}_s$ is given by

$$\boldsymbol{\Psi}_s(z,s) = \begin{pmatrix} \mathbf{E}_z(\mathbf{d},\mathbf{h},z,s) - \mathbf{E}_z(\mathbf{d},\mathbf{0},z,s) + \frac{\partial \mathbf{V}^e}{\partial z}(z,s) \\ \mathbf{Y}(s)\mathbf{V}^e(z,s) \end{pmatrix}. \tag{20}$$

The general solution to equation (18) can be written as follows:

$$\boldsymbol{\Psi}(z,s) = \exp(-A(s)z)\left(\int_0^z \exp(Az')\boldsymbol{\Psi}_s(z',s)\,\mathrm{d}z' + \boldsymbol{\Psi}(0,s)\right). \tag{21}$$

Let

$$\int_0^z \exp(Az')\boldsymbol{\Psi}_s(z',s)\,\mathrm{d}z' = \begin{pmatrix} \mathbf{Q}_v(z,s) \\ \mathbf{Q}_I(z,s) \end{pmatrix} \tag{22}$$

where $\mathbf{Q}_v$ and $\mathbf{Q}_I$ are N-dimensional column vectors. Since the z dependence of the exciting electric field is characterized by an exponential term (see equations (15), (16)), analytical expressions for $\mathbf{Q}_v$ and $\mathbf{Q}_I$ are simply given by

$$\begin{pmatrix} \mathbf{Q}_v(z,s) \\ \mathbf{Q}_I(z,s) \end{pmatrix} = (\mathbf{A} - \xi_{\theta,\phi}(s)\mathbf{U})^{-1}(\exp((\mathbf{A} - \xi_{\theta,\phi}(s)\mathbf{U})z) - \mathbf{U})\boldsymbol{\Psi}_s(0,s)$$

where $\xi_{\theta,\phi}(s) = s/v\cos(\theta)\cos(\phi)$ and $\mathbf{U}$ is the unit matrix of dimension $2N \times 2N$.

It can easily be seen from equations (21) and (22) that the currents and voltages at the line ends obey the following relationship:

$$\begin{pmatrix} \mathbf{I}(0,s) \\ -\mathbf{I}(l,s) \end{pmatrix} = \tilde{\mathbf{Y}}\begin{pmatrix} \mathbf{V}(0,s) \\ \mathbf{V}(l,s) \end{pmatrix} + \tilde{\mathbf{Y}}\begin{pmatrix} \mathbf{Q}_v(l,s) \\ \mathbf{0} \end{pmatrix} - \begin{pmatrix} \mathbf{Q}_I(l,s) \\ \mathbf{0} \end{pmatrix} \tag{23}$$

where the N-dimensional elements $\tilde{\mathbf{Y}}_{ij}$ $(i, j = 1, 2)$ of the admittance matrix $\tilde{\mathbf{Y}}$ are given by

$$\tilde{\mathbf{Y}} = \begin{pmatrix} \tilde{\mathbf{Y}}_{11} & \tilde{\mathbf{Y}}_{12} \\ \tilde{\mathbf{Y}}_{12} & \tilde{\mathbf{Y}}_{22} \end{pmatrix} \qquad \tilde{\mathbf{Y}}_{11} = \tilde{\mathbf{Y}}_{22} = -\mathbf{K}_{12}^{-1}\mathbf{K}_{11} \qquad \tilde{\mathbf{Y}}_{12} = \tilde{\mathbf{Y}}_{21} = \mathbf{K}_{12}^{-1}$$

with $\exp(-A(s)l) = \begin{pmatrix} \mathbf{K}_{11} & \mathbf{K}_{12} \\ \mathbf{K}_{21} & \mathbf{K}_{22} \end{pmatrix}$.

Since the loads at the near end ($z = 0$) of the line are linear time-invariant resistors (figure 2), it can readily be shown that

$$\mathbf{V}(0,s) = -\mathbf{R}\mathbf{I}(0,s) \tag{24}$$

where $\mathbf{R} = R\mathbf{U}$.

To deal with nonlinear components at the far end ($z = l$) line terminals, it is convenient and more illuminating to rewrite equations (23) and (24) in a single matrix equation as follows,

$$\hat{\mathbf{A}}(s)\boldsymbol{\chi}(s) = \mathbf{W}_s(s) - \mathbf{D}\mathbf{I}(l,s) \tag{25}$$

where

$$\hat{\mathbf{A}}(s) = \begin{pmatrix} \tilde{\mathbf{Y}} & & -\mathbf{U} \\ & & \mathbf{0} \\ \mathbf{U} & \mathbf{0} & \mathbf{R} \end{pmatrix}$$

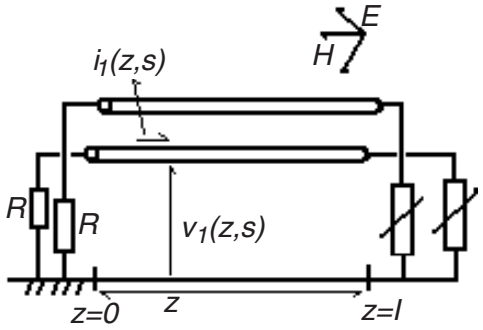

Figure 2. Nonlinear loaded transmission line.

$$\mathbf{W}_s(s) = \left(\begin{bmatrix} \mathbf{Q}_I(l,s) \\ \mathbf{0} \end{bmatrix} - \tilde{\mathbf{Y}} \begin{bmatrix} \mathbf{Q}_v(l,s) \\ \mathbf{0} \end{bmatrix} \right)_{\mathbf{0}}$$

$$\mathbf{D} = (\mathbf{0}, \mathbf{U}, \mathbf{0})^T \qquad \boldsymbol{\chi}(s) = (\mathbf{V}(0,s), \mathbf{V}(l,s), \mathbf{I}(0,s))^T.$$

It is important to note here that the nonlinear load currents, $\mathbf{I}(l,s)$, must be sorted out and displayed, prominently, on the right-hand side of the equation.

Now, using the piecewise-linear approximation stipulated in equation (17), the nonlinear (VCCS) $\mathbf{I}(l,\tau)$ at any time τ of the interval of analysis $[0,T]$ may be written as

$$\mathbf{I}(l,\tau) = \Delta \sum_{k=0}^{M-1} \mathbf{I}_k P_\Delta(\tau - \tau_k) + \sum_{k=0}^{M-1} (\mathbf{I}_{k+1} - \mathbf{I}_k) r_\Delta(\tau - \tau_k) \tag{26}$$

where $r_\Delta(\tau) = \tau P_\Delta(\tau)$ and $\mathbf{I}_k = \mathbf{I}(l,\tau_k)$.

On inserting the Laplace transform of $\mathbf{I}(l,\tau)$ in equation (25), one can easily check that

$$\boldsymbol{\chi}(s) = \boldsymbol{\chi}_s(s) - \Delta \boldsymbol{\chi}_{P_\Delta}(s) \sum_{k=0}^{M-1} \mathbf{I}_k \exp(\tau_k s) - \boldsymbol{\chi}_{r_\Delta}(s) \sum_{k=0}^{M-1} (\mathbf{I}_{k+1} - \mathbf{I}_k) \exp(\tau_k s) \tag{27}$$

where

$$\boldsymbol{\chi}_s(s) = \hat{\mathbf{A}}^{-1}(s)\mathbf{W}_s(s)$$
$$\boldsymbol{\chi}_{P_\Delta}(s) = \hat{\mathbf{A}}^{-1}(s)\mathbf{D}\mathcal{L}(p_\Delta(\tau))$$
$$\boldsymbol{\chi}_{P_\Delta}(s) = \hat{\mathbf{A}}^{-1}(s)\mathbf{D}\mathcal{L}(r_\Delta(\tau))$$

with $\mathcal{L}$ denoting the operation of taking the Laplace transform. The operation of going back to the time domain from the Laplace domain will be denoted by $\mathcal{L}^{-1}$.

3.3. Numerical inversion of Laplace transform

Many conventional algorithms for numerical inversion of Laplace transforms are based on the complex inversion formula [13]

$$\boldsymbol{\chi}(t) = \frac{1}{2\pi \mathbf{i}} \int_{c-\mathbf{i}\infty}^{c+\mathbf{i}\infty} \boldsymbol{\chi}(s)\, \mathrm{e}^{st}\, \mathrm{d}s \qquad t \geqslant 0 \tag{28}$$

where $\boldsymbol{\chi}(t)$ satisfies an inequality of the form ($|\boldsymbol{\chi}(t)| < F\, \mathrm{e}^{\sigma t}$ $(t \to \infty)$) and $\boldsymbol{\chi}(s)$ is defined for all values of s lying in a half-plane $\mathrm{Re}(s) > \sigma$. Under these assumptions, an approximate

formula of (28) in discrete form can be written as

$$\Phi_k \approx \frac{\omega}{2\pi}\exp(c\tau_k)\left(2\mathrm{Re}\left(\sum_{n=0}^{N_L-1}\chi(c-\mathbf{i}n\omega)\exp(-\mathbf{i}\tau_k n\omega)\right)-\chi(c)\right)$$
$$k=0,1,\ldots,N_L-1 \tag{29}$$

$$\chi(\tau_k)=[\Phi_k]_M \tag{30}$$

where $\omega=\frac{\pi}{T}$, $\tau_k=k\Delta$ and $N_L=2M$. The coefficient c can be set using the formula

$$c\approx\sigma-\frac{\omega}{2\pi}\ln(\varepsilon) \tag{31}$$

where ε denotes the desired relative error.

The evaluation of the sum in equation (29) is performed using the *FFT* algorithm [14] which is particularly useful since it offers the saving of a significant number of numerical operations over conventional methods. The operator $[.]_M$ designates the first M elements of the *FFT* operation result. In other words, $k=0,1,\ldots,M-1$ in equation (30). It should be remarked, at this point, that in practice an increasing error at the end of the interval $[0,T]$ occurs when one uses relationship (30). This error occurs as a result of working with a finite sum (29) which should be normally infinite. To minimize this error, the u-nonlinear transformation which requires a few additional terms above those N_L terms used by the *FFT* algorithm is applied to give a precision to the resultant sum. To this end, let

$$\mathbf{a}_\chi(1)=\left[\sum_{n=0}^{N_L-1}\chi(c-\mathbf{i}n\omega)\,\mathrm{e}^{-\mathbf{i}\tau_k n\omega}\right]_M$$
$$\mathbf{a}_\chi(j)=\chi(c-\mathbf{i}(N_L+j-2)\omega)\exp(-\mathbf{i}\tau_k(N_L+j-2)\omega) \tag{32}$$
$$j=2,3,\ldots,N_u \qquad k=0,2,\ldots,M-1.$$

The u-transformation [15] is defined by

$$\mathbf{u}_\chi=\left(\sum_{j=0}^{N_u}(-1)^j\binom{N_u}{j}\left(\frac{1+j}{N_u+1}\right)^{(N_u-2)}\mathbf{A}_\chi(1+j)/\mathbf{a}_\chi(1+j)\right)\Bigg/$$
$$\left(\sum_{j=0}^{N_u}(-1)^j\binom{N_u}{j}\left(\frac{1+j}{N_u+1}\right)^{(N_u-2)}1/\mathbf{a}_\chi(1+j)\right) \tag{33}$$

and $\mathbf{A}_\chi(m)=\sum_{j=1}^{m}\mathbf{a}_\chi(j)$. The operator / denotes element-by-element division. Practically, one gets better accuracy of the results by setting $N_u=5$ or 7. The proposed formula for the numerical inverse Laplace transform is then given by

$$\chi(\tau_k)=\frac{\omega}{2\pi}\,\mathrm{e}^{c\tau_k}(2\,\mathrm{Re}\,(\mathbf{u}_{\chi_k})-\chi(c)) \qquad k=0,1,\ldots,M-1 \tag{34}$$

where $\mathbf{u}_{\chi_k}$ is the kth element of $\mathbf{u}_\chi$.

To illustrate the loss of accuracy in the computation of $\chi(\tau)$ using equation (30), let us consider, as an example, $\chi(s)=\frac{1}{s}\frac{1+\mathrm{e}^{-2s}}{1-\mathrm{e}^{-2s}}$. The inverse Laplace transform of $\chi(s)$ is given in the following closed-form $\chi(\tau)=\tau+\frac{2}{\pi}\sum_{n=1}^{\infty}\frac{\sin(n\pi\tau)}{n}$. A plot of $\mathcal{L}^{-1}(\chi(s))$ obtained from equations (30) and (34) is given in figure 3. As indicated, there is a progressive loss of accuracy with increasing time for equation (30).

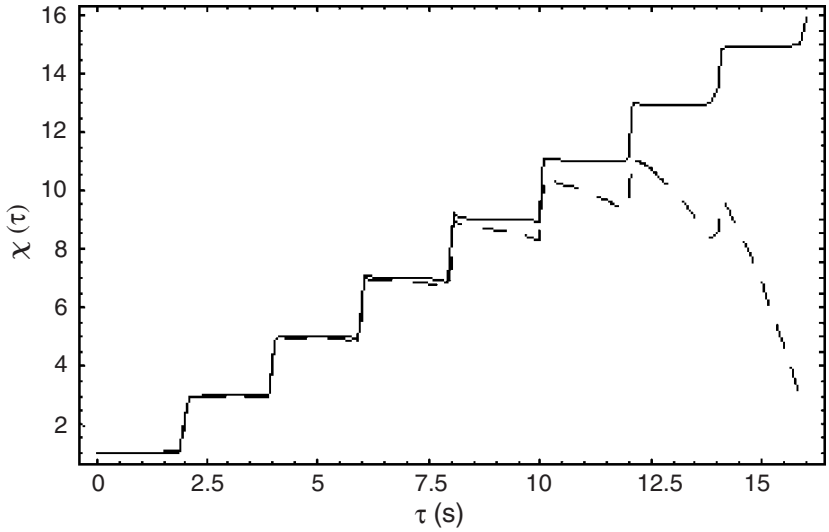

Figure 3. Comparison of numerical inverse Laplace transforms using equation (30) (dashed) and equation (34) (solid).

3.4. Time-domain response and numerical examples

Let $\mathcal{L}^{-1}(\boldsymbol{\chi}(s), \boldsymbol{\chi}_{p_\Delta}(s), \boldsymbol{\chi}_{r_\Delta}(s)) = (\boldsymbol{\chi}(\tau), \boldsymbol{\chi}_{p_\Delta}(\tau), \boldsymbol{\chi}_{r_\Delta}(\tau))$. It is easy to show from equation (27) that

$$\boldsymbol{\chi}(\tau) = \boldsymbol{\chi}_s(\tau) - \Delta \sum_{k=0}^{M-1} \boldsymbol{\chi}_{P_\Delta}(\tau - \tau_k)\mathbf{I}_k - \sum_{k=0}^{M-1} \boldsymbol{\chi}_{r_\Delta}(\tau - \tau_k)(\mathbf{I}_{k+1} - \mathbf{I}_k). \tag{35}$$

The voltage and current at the line far end are obtained by solving a set of M nonlinear algebraic equations in the time domain in the form

$$\mathbf{f}(\mathbf{D}\boldsymbol{\chi}(t_r)) - \mathbf{I}(l, t_r) = 0 \qquad r = 0, 1, \ldots, M-1 \tag{36}$$

where $\tau_r < t_r < \tau_{r+1}$ and $\Delta = t_{r+1} - t_r$ $(r = 0, 1, \ldots, M-1)$. Using (35), $\boldsymbol{\chi}(t_r)$ may be expressed as

$$\boldsymbol{\chi}(t_r) = \boldsymbol{\alpha}_\chi^r \mathbf{I}_{r+1} + \boldsymbol{\beta}_\chi^r \tag{37}$$

with

$$\begin{aligned} \boldsymbol{\alpha}_\chi^r &= -\boldsymbol{\chi}_{r_\Delta}(t_r - \tau_r) \\ \boldsymbol{\beta}_\chi^r &= \sum_{k=0}^{r} (\boldsymbol{\chi}_{r_\Delta}(t_r - \tau_k) - \Delta \boldsymbol{\chi}_{P_\Delta}(t_r - \tau_k))\mathbf{I}_k + \boldsymbol{\chi}_s(t_r) - \sum_{k=0}^{r-1} \boldsymbol{\chi}_{r_\Delta}(t_r - \tau_k)\mathbf{I}_{k+1}. \end{aligned} \tag{38}$$

The formula from which the updated vector $\mathbf{I}_{r+1}^{(j+1)}$ is calculated in Newton's iteration is

$$\begin{aligned} &\mathbf{J}|_{\mathbf{I}_{r+1}=\mathbf{I}_{r+1}^{(j)}} \left(\mathbf{I}_{r+1}^{(j+1)} - \mathbf{I}_{r+1}^{(j)}\right) = -(\mathbf{f}(\mathbf{D}\boldsymbol{\chi}^{(j)}(t_r)) - \mathbf{I}^{(j)}(l, t_r)) \\ &\mathbf{J}|_{\mathbf{I}_{r+1}=\mathbf{I}_{r+1}^{(j)}} = \frac{\partial \mathbf{f}(\mathbf{v})}{\partial \mathbf{v}} \mathbf{D}\alpha_\chi^r - \frac{t_r - \tau_r}{\Delta}\mathbf{U} \qquad \mathbf{v} = \mathbf{D}\boldsymbol{\chi}. \end{aligned} \tag{39}$$

The iteration is continued until $\mathbf{I}_{r+1}^{(j+1)}$ and $\mathbf{I}_{r+1}^{(j)}$ are sufficiently close to each other.

As an example of the responses provided by this calculational model, a bifilar transmission line described in figure 2 has been considered. The metal oxide varistors (MOVs) are used as

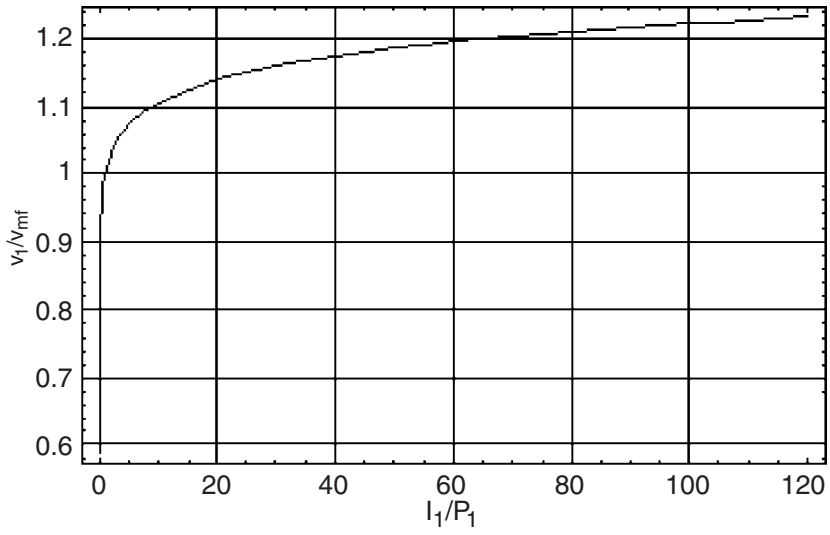

Figure 4. MOV characteristics.

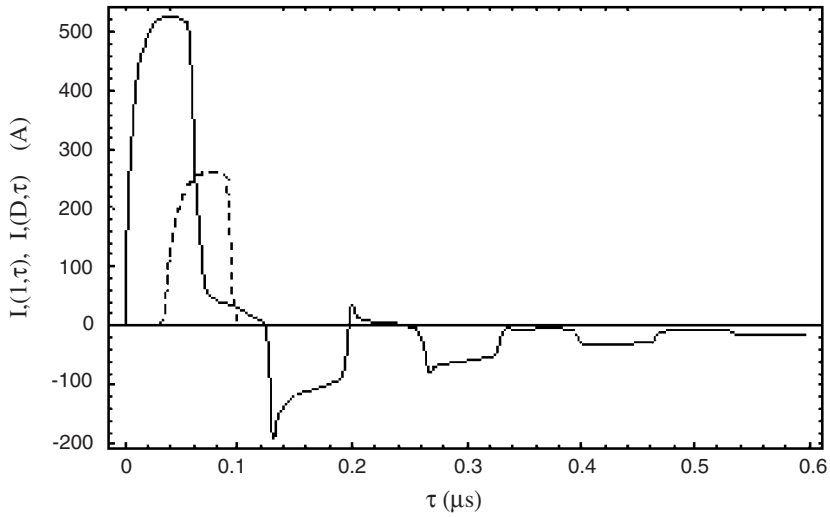

Figure 5. Near end (solid) and far end (dashed) line currents.

nonlinear components of the network. The MOVs with the common approximation of the v–i characteristics (figure 4) were taken:

$$\mathbf{I}(l,\tau) = \mathbf{f}(\mathbf{D}\chi) = (f_1(V_1(l,\tau), f_2(V_2(l,\tau))^T$$
$$f_i(v) = P_i\left(\frac{v}{v_{\text{ref}}^{(i)}}\right)^{q_i} \qquad i = 1,2 \tag{40}$$

where $P_{1,2} = 1\,\text{kA}$, $q_{1,2} = 23$ and $v_{\text{ref}}^{(1,2)} = 150\,\text{kV}$.

The pulse $E(\tau)$ is assumed to be a bi-exponential function

$$E(\tau) = E_o(\mathrm{e}^{-\alpha\tau} - \mathrm{e}^{-\beta\tau})$$

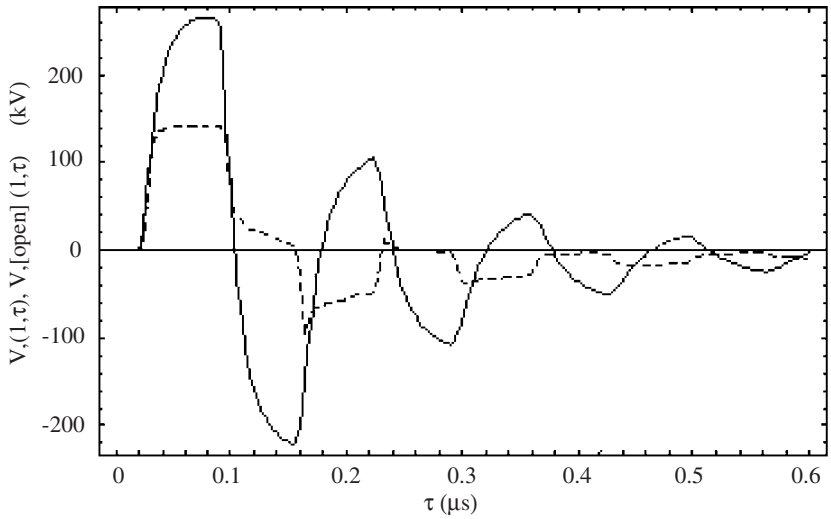

Figure 6. Transient induced voltages at the line terminals. The solid curve represents the open-circuit voltage. The nonlinear load voltage is specified by the dashed curve.

where $E_o = 56.6$ kV m^{-1}, $\alpha = 4.086 \times 10^6\,\mathrm{s}^{-1}$, $\beta = 1.56 \times 10^8$ s^{-1}. Ground resistivity and permittivity are $100\,\Omega$ m and 15 respectively. The following values are assigned to the parameters of the impinging plane wave: $\phi = 0^\circ$, $\eta = 0^\circ$ and $\theta = 30^\circ$. The value of the linear resistor is $R = 100\,\Omega$.

The curves in figure 5 correspond to the currents at the line terminals. These currents are calculated using $N_L = 128$ frequency points.

An examination of figure 6 shows that the voltage at the end of the line does not exceed 150 kV. This is exactly the value of the voltage v_{ref} specified by the nonlinear component. Also shown is a decrease in oscillations caused by the nonlinear surge arrester.

4. Conclusion

A new approach for calculating transients in lossy line systems exposed to external fields has been presented. Analysis of the multiconductor system based on the transmission line theory is performed by considering equivalent circuits in which induced voltages and currents are calculated as a function of the series impedance and the shunt admittance of the line. Losses in the ground are taken into account by introducing an accurate analytical expression for these transmission line parameters. The formulation of the network equations is performed in the Laplace s-domain. The nonlinear loads are replaced by time-dependent sources using the linear-piecewise approximation. The time-domain results are obtained using an accurate FFT-based numerical inverse Laplace transform in conjunction with the u -nonlinear transformation and Newton's algorithm.

References

[1] Vance E F 1978 *Coupling to Shielded Cables* (New York: Wiley–Interscience.)
[2] Ianoz M, Nucci C A and Teshe F M 1988 Transmission line coupling for field-to-transmission line calculations *Electromagnetics* **8** 171–211

[3] Paul C R 1976 Frequency response of multi-conductor transmission lines illuminated by an electromagnetic field *IEEE Trans. Electromagn. Compat.* **18** 183–90
[4] Maaouni A and Amri A 2002 Overhead line switching transients *J. Phys. A: Math. Gen.* **35** 7125–35
[5] Haase H and Nitsch J 2003 Investigation of nonuniform transmission line structures by a generalized transmission-line theory *Proc. EMC Sym. Zurich* pp 597–602
[6] Djordjevic A R, Sarkar T K and Harrington R F 1987 Time-domain response of multiconductor transmission lines *Proc. IEEE* **75** 743–64
[7] Bouchard P and Gagné R R J 1995 Transient analysis of lossy parabolic transmission lines with nonlinear loads *IEEE Trans. Microw. Theory. Tech.* **43** 1330–33
[8] Yeung P S 1993 Lossy transmission lines: time domain formulation and simulation model *IEEE Trans. Microw. Theory. Tech.* **41** 1275–9
[9] Rachidi F 1993 Formulation of the field to transmission line coupling equations in terms of magnetic excitation field *IEEE Trans. Electromagn. Compat.* **35** 404–7
[10] Maaouni A, Amri A and Zouhir A 2001 Simple and accurate analytical expressions for evaluating related transmission line integrals *J. Phys. A: Math. Gen.* **34** 9027–35
[11] Abramowitz M and Stegun I 1964 *Handbook of Mathematical Functions* (Washington, DC: National Bureau of Standards)
[12] Wait J R 1987 *Electromagnetic Wave Theory* (New York: Wiley)
[13] Davies B and Martin B 1979 Numerical inversion of Laplace transform: survey and comparison of methods *J. Comput. Phys.* **33** 1–32
[14] Cooley J W and Tukey J W 1965 An algorithm for the machine calculation of complex Fourier series *Math. Comput.* **19** 297–301
[15] Levin D 1973 Development of non-linear transformations for improving convergence of sequences *Int. J. Comput. Math.* B **3** 371–88